Strain assessment in the carotid artery wall using ultrasound speckle tracking: validation in a sheep model

Strain assessment in the carotid artery wall using ultrasound speckle tracking: validation in a sheep model

Matilda Larsson[1,2]**, Peter Verbrugghe**[3]**, Marija Smoljkić**[4]**,
Jelle Verhoeven**[3]**, Brecht Heyde**[2]**, Nele Famaey**[4]**,
Paul Herijgers**[3] **and Jan D'hooge**[2]

[1] Department of Medical Engineering, KTH Royal Institute of Technology, Stockholm, Sweden
[2] Lab on Cardiovascular Imaging and Dynamics, KU Leuven—University of Leuven, Leuven, Belgium
[3] Department of Cardiovascular Sciences, KU Leuven—University of Leuven, Leuven, Belgium
[4] Biomechanics Section, Department of Mechanical Engineering, KU Leuven—University of Leuven, Leuven, Belgium

E-mail: matilda.larsson@sth.kth.se

CrossMark

Abstract

The aim of this study was to validate carotid artery strain assessment *in-vivo* using ultrasound speckle tracking. The left carotid artery of five sheep was exposed and sonomicrometry crystals were sutured onto the artery wall to obtain reference strain. Ultrasound imaging was performed at baseline and stress, followed by strain estimation using an in-house speckle tracking algorithm tuned for vascular applications. The correlation between estimated and reference strain was $r = 0.95$ ($p < 0.001$) and $r = 0.87$ ($p < 0.01$) for longitudinal and circumferential strain, respectively. Moreover, acceptable limits of agreement were found in Bland–Altman analysis (longitudinally: −0.15 to 0.42%, circumferentially: −0.54 to 0.50%), which demonstrates the feasibility of estimating carotid artery strain using ultrasound speckle tracking. However, further studies are needed to test the algorithm on human *in-vivo* data and to investigate its potential to detect subclinical cardiovascular disease and characterize atherosclerotic plaques.

1. Introduction

Early detection in combination with risk stratification is essential to initiate appropriate treatment strategies and improve prognosis of cardiovascular disease. Several known risk factors, such as smoking, hypertension and diabetes, and elevated arterial stiffness are strongly associated with cardiovascular morbidity (Yusuf *et al* 2004, Sutton-Tyrrell *et al* 2005, Hae Guen *et al* 2010). Arterial stiffness is regarded as an indicator of subclinical cardiovascular disease and thus crucial to assess for detection of disease at an early stage. Moreover, methods for refined risk stratification are needed in patients with established atherosclerotic disease to identify at-risk patients with vulnerable plaques that are prone to rupture and cause acute ischemic events.

Some existing indices of arterial stiffness that have been associated with cardiovascular risk are pulse wave velocity (Sutton-Tyrrell *et al* 2005, Hermeling *et al* 2007), arterial distensibility (Hoeks *et al* 1990, Redheuil *et al* 2010) and β-stiffness index (Eryol *et al* 2002). However, the clinical significance of these methods remains uncertain and a standardized method assessing arterial stiffness in a reproducible manner is still missing. Current clinical practice to determine suitability of patients with plaques for surgery, rely on visual assessment and estimation of the percentage of the flow limiting stenosis (NASCET 1991). However, recent studies show that plaque rupture and thrombosis, rather than the stenosis, precipitate most acute ischemic events (Naghavi *et al* 2003). Methods for improved risk stratification are thus needed to identify plaques at high risk of rupture, which in recent studies have been characterized by active inflammation, large lipid core, thin fibrous cap, intraplaque hemorrhage, and neovascularization of the vasa vasorum (Falk *et al* 1995, Naghavi *et al* 2003, Fleiner *et al* 2004, Staub *et al* 2010).

During the last decade, methods for estimation of arterial wall motion and strain have become more common in the assessment of arterial stiffness and plaque characteristics. Arterial strain has shown potential in subclinical detection of increased arterial stiffness, since correlations were found between circumferential strain and conventional indices of arterial stiffness (Catalano *et al* 2011), and between radial strain and cardiovascular risk score (Kawasaki *et al* 2009). Moreover, arterial strain distribution has been correlated with histological composition of atherosclerotic arteries in pigs (de Korte *et al* 2002, Liang *et al* 2009), which demonstrates that arterial strain measurements are promising also for assessment of plaque vulnerability to predict plaque rupture.

Ultrasound speckle tracking is a technique that allows for tissue motion and strain estimation by tracking interference patterns across imaging frames. The technique has mainly been developed for assessment in the myocardium (D'hooge *et al* 2002) but has also been applied in other applications such as tendon strain assessment (Korstanje *et al* 2010). Strain estimation in the arterial wall and in atherosclerotic plaques is particularly challenging because of the small structures involved and their low physiologic deformation in relation to the applied ultrasound wavelength used in clinical ultrasound systems. The feasibility of radial and circumferential arterial strain estimation has been demonstrated both *in-vitro* and *in-vivo* (Ribbers *et al* 2007, Schmitt *et al* 2007, Hansen *et al* 2009, Kawasaki *et al* 2009, Redheuil *et al* 2010, Korukonda and Doyley 2012, McCormick *et al* 2012), whereas the feasibility to assess motion and strain

along the longitudinal axis of the arterial wall has been investigated less (Cinthio *et al* 2005, Mahmoud *et al* 2009, Larsson *et al* 2011). In contrast to circumferential and radial motion, the longitudinal motion of the arterial wall is more difficult to assess due to low amplitudes combined with the intrinsic lower spatial resolution in the azimuth direction of the ultrasound image. However, improved imaging techniques have allowed estimation of arterial longitudinal motion using different ultrasound speckle tracking approaches (Golemati *et al* 2003, Persson *et al* 2003) and it has been demonstrated to be of the same magnitude as the radial movement (Cinthio *et al* 2006). Moreover, it has been shown that the longitudinal motion of the artery may be an important factor in early detection of cardiovascular diseases (Zahnd *et al* 2012). Recent findings also associate reduced longitudinal wall motion with plaque burden (Svedlund and Gan 2011) and potential to predict cardiovascular outcome (Svedlund *et al* 2011), which indicates that the arterial longitudinal function is an important contributor in the evaluation of cardiovascular diseases.

Recently, we developed an ultrasound speckle tracking algorithm with parameters tuned for the vascular setting (Larsson *et al* 2011). The feasibility of the algorithm to assess carotid radial and longitudinal strain based on simulated ultrasound data sets was shown (Larsson *et al* 2011). Moreover, radial, longitudinal and circumferential strain estimation was validated with promising results via sonomicrometry in data sets from dynamic gel phantoms (Larsson *et al* 2015). Even though the potential of arterial strain imaging has been demonstrated by applying different speckle tracking techniques *in-silico* and *in-vitro*, the results from strain estimation in simulations and phantoms cannot directly be translated to the *in-vivo* setting, which is likely more challenging, given that more artefacts due to e.g. patient and transducer motion may be present. A thorough validation study of arterial strain assessment by ultrasound speckle tracking via an independent method *in-vivo* is still missing. Accordingly, the aim of this study was to validate strain assessment in the carotid artery wall by ultrasound speckle tracking in an animal setup.

2. Methods

A carotid sheep model was developed to validate the ultrasound speckle tracking algorithm via sonomicrometry. Radial, longitudinal and circumferential strain of the left common carotid artery of five sheep was estimated by speckle tracking before and after the attachment of sonomicrometry crystals on the artery wall. Longitudinal and circumferential strain obtained after attachment of crystals at baseline and induced hypertension was then compared with reference strain by sonomicrometry. Hypertension was induced in order to obtain a sufficient range of strain values for the validation.

2.1. Animal preparation

The experiments obtained ethical approval (EC n°: P160-2010) from the local ethics committee (Animal Ethics Committee of KU Leuven, Leuven, Belgium) and were performed in concordance to the Guide for the Care and Use of Laboratory Animals published by the U.S. National Institutes of Health (NIH Publication No. 85-23, revised 1996). Five 1 year-old female Swifter sheep were included in the study. The sheep were pre-sedated with an intramuscular injection of Ketamine ($15 \, mg \, kg^{-1}$) and xylazine (2%, $0.01 \, ml \, kg^{-1}$). Anesthesia was induced with Isoflurane (5%) and the trachea of the animal was intubated. Anesthesia was maintained throughout the procedure with an isoflurane (2–4%)–oxygen (50%) mixture, mechanically ventilated at a respiratory rate of 12 cycles per minute. An intravenous line was

Table 1. Characteristics of the five 1 year-old female Swifter sheep included in the study.

	Weight (kg)	Heart rate baseline/ hypertension (bpm)	BP—Baseline systolic/ diastolic (mmHg)	BP—Hypertension systolic/diastolic (mmHg)
Sheep #1	45	74/220	84/64	172/78
Sheep #2	54	66/180	95/80	140/108
Sheep #3	51	66/76	83/64	210/165
Sheep #4	44	70/127	74/56	136/111
Sheep #5	49	75/111	75/50	168/136

BP: blood pressure.

inserted in an extremity vein and an arterial line in the ear to allow drug administration and pressure measurements, respectively. Heart rate, blood pressure, end-tidal CO_2, and blood O_2-saturation were constantly monitored throughout the procedure. Characteristics of the animals are presented in table 1.

The animals were positioned in supine position on a surgical table with a neck extension of 180°. A 5 cm long longitudinal incision was made to expose the left common carotid artery approximately 2.5 cm distal to the carotid bifurcation, see figure 1(*b*). A digital sonomi-crometry system (Sonometrics Corporation, London, ON, Canada) was used to obtain reference values of circumferential and longitudinal strain. Five sonomicrometry crystals with a diameter of 1 mm were attached with suture prolene 6/0 to the adventitia of the proximal and distal carotid artery wall according to figures 1(*a*) and (*b*). To allow ultrasound imaging in the long-axis plane perpendicular to the skin without visible crystals in the image, the crystals were positioned slightly out of this plane as visualized in figure 1(*b*). The crystals were stitched with an inter-crystal distance of approximately 5–7 mm, with three crystals at the top of the artery (c_1, c_2, c_3) and two crystals on the opposite side of the artery 180° apart in the short-axis view (c_4, c_5). The incision was then closed in layers and filled with ultrasound gel and saline solution. To obtain a range of strain values for the validation, hypertension was induced with infusion of Phenylephrine ($3 \mu g \, kg^{-1} \, min^{-1}$) during data acquisition. The hypertension was expected to result in larger pulse pressures and thus larger strain values than at baseline.

2.2. Data acquisition

Ultrasound data were collected at baseline before opening the neck and exposing the artery and at baseline and induced hypertension after wound closure. The time between crystal positioning and data acquisition after wound closure was approximately 10–15 min. Ultrasound long-axis and short-axis images of the left common carotid artery were acquired using a Vivid7 system (GE Healthcare, Horten, Norway) with a linear-array transducer (12L) at a center frequency of 12 MHz and a sampling frequency of 40 MHz. Images were acquired throughout three cardiac cycles in long-axis and short-axis planes using free-hand scanning. The long-axis views were obtained in the long-axis plane perpendicular to the skin, i.e. slightly rotated from the crystal plane. The short-axis views were obtained in the short-axis plane just parallel to the positions of the sonomicrometry crystals towards the head, i.e. to the right of the crystals in figure 1. The images were acquired at a frame rate of $45.3 \, \text{frames} \, s^{-1}$ with a line density of $13.9 \, \text{lines} \, mm^{-1}$ in the grayscale image. The image depth was 30 mm, whereas the image width was 27 mm. The focus point was positioned in the posterior wall of the artery. Figure 2 shows example grayscale long-axis and short-axis images of the left
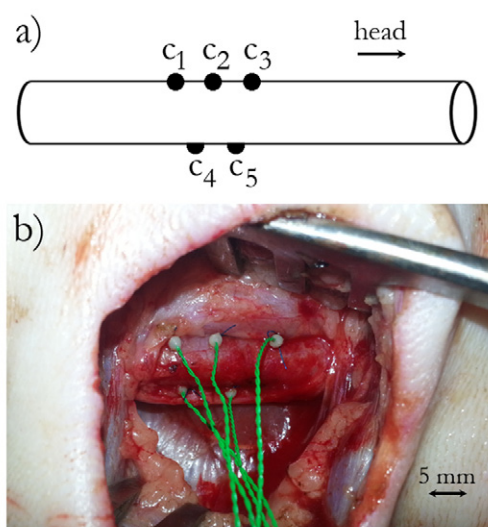
Figure 1. (*a*) Schematic illustration of the left common carotid artery with positions of sonomicrometry crystals (solid circles c_1–c_5). (*b*) Photo of exposed left common carotid artery with five attached sonomicrometry crystals.
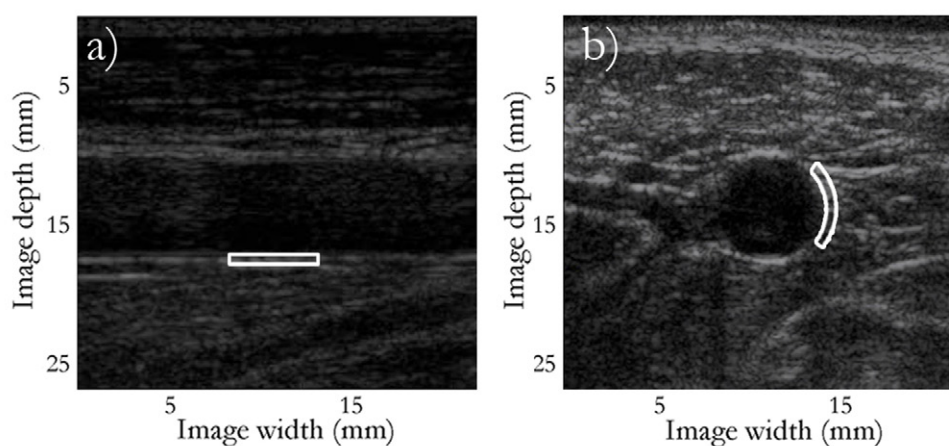

Figure 2. Ultrasound long-axis (*a*) and short-axis (*b*) images in end-diastole of the left common carotid artery. The white boxes represent the region of interest (ROI) for longitudinal strain (*a*) and circumferential strain (*b*). The ROI for radial strain estimation was positioned in the center of the ROI for longitudinal strain estimation. The images have been slightly zoomed for better visualization.

common carotid artery in one of the animals. ECG was registered using needle electrodes connected to the ultrasound system.

Sonomicrometry data for reference strain calculation were acquired after wound closure at baseline and induced hypertension using the sonomicrometry system (Sonometrics Corporation, London, ON, Canada). The data were collected at a sampling rate of 1 kHz

throughout six cardiac cycles. Sonomicrometry data and ultrasound images were recorded in randomized order and only one of the systems was active simultaneously in order to avoid sound interference.

2.3. Data analysis

The collected data were analyzed offline using in-house developed Matlab (R2010a, MathWorks, Natick, MA, USA) software. Speckle tracking analysis was performed on the ultrasound images and the inter-crystal distances were processed to assess values of reference strain.

2.3.1. Speckle tracking analysis

Speckle tracking analysis was performed on the envelope-detected data throughout three consecutive cardiac cycles using the previously developed algorithm with similar motion estimation parameters (Larsson *et al* 2011), where one cardiac cycle was identified as the interval between two R-waves in the ECG. Two-dimensional (2D) motion estimation was performed across subsequent frames using normalized cross-correlation (kernel width: 5 wavelengths (λ) ≈ 0.64 mm, kernel length: $2\lambda \approx 0.26$ mm, 40% axial and lateral overlap, spline interpolation for detection of sub-sample motion). To remove outliers, the motion estimates were filtered by applying a 2D median filter on a region of 0.08 mm (axial) by 0.3 mm (lateral). This was followed by linear interpolation between samples to obtain motion estimates in the entire image. The displacement maps were then cumulated throughout the cardiac cycle using linear interpolation to account for sub-pixel motion.

Radial (i.e. perpendicular to the flow direction) and longitudinal strains (i.e. along the flow direction) were estimated in the ultrasound long-axis images throughout three consecutive cardiac cycles in regions of interest (ROI). For each cardiac cycle, the ROI was manually positioned in the middle of the posterior artery wall close to the position of the crystals, see figure 2(*a*). The ROI width was 3 mm and ROI length 0.5 mm when calculating radial strains, whereas the ROI width was 6 mm and the ROI length 1 mm when calculating longitudinal strains. The ROIs were placed to mainly cover the intima-media complex of the wall (≈ 0.5–0.6 mm) and the upper parts of the adventitia. For calculation of circumferential strain, the lateral and axial displacement maps in the short-axis views were converted into polar coordinates. Strains were estimated throughout three consecutive cardiac cycles, in a circular ROI positioned in the middle of the arterial wall at 3 o'clock (radial ROI size = 0.5 mm, circumferential ROI size = 90°), see figure 2(*b*). The strain values were obtained by spatial linear regression after averaging the cumulated displacement maps in one direction of the ROI, i.e. radially for longitudinal strain, longitudinally for radial strain and radially for circumferential strain.

Drift compensation was then applied on the strain curves to obtain values of zero strain at the end of each cardiac cycle. The drift compensated strain (ε_{DC}) in frame *t* was calculated as:

$$\varepsilon_{DC}(t) = \varepsilon(t) - \frac{\sum_{i=1}^{t} |\varepsilon(i) - \varepsilon(i-1)|}{\sum_{j=1}^{T} |\varepsilon(j) - \varepsilon(j-1)|} \varepsilon(T), \tag{1}$$

where frame 1 was the first frame and frame T the last frame in the cardiac cycle (Kremer *et al* 2010). After drift compensation, the strain curves were low-pass filtered in order to remove noise, by convolving the curves with a normalized rectangular function of 5 time samples in length.

2.3.2. Reference strain calculation

Depending on signal quality, only three of the attached crystals in figure 1(*a*) were selected for further analysis. The reason for attaching several crystals on the artery wall was to be able to choose crystals in case of poor signal quality between some of the crystal pairs. The inter-crystal displacement between crystal c_4 and c_5 (D_L) was processed to obtain reference longitudinal strain, and inter-crystal displacement between crystal c_2 and c_5 (D_C) to obtain reference circumferential strain, see figure 1(*a*). Reference radial strain could not be obtained, since the attachment of a crystal inside the vessel lumen was not possible. The inter-crystal displacements were median filtered with a filter length of 35 ms to reduce noise and then averaged over six cycles to account for any physiological change during the acquisition. Longitudinal and circumferential strain (ε) was then calculated throughout one cycle as:

$$\varepsilon_i(t) = \left(\frac{D_i(t) - D_i(t_o)}{D_i(t_o)} \right), \tag{2}$$

where $D_i(t_0)$ was the inter-crystal displacement at the start of the cardiac cycle and $D_i(t)$ the inter-crystal displacement at time point t for longitudinal strain estimation ($i = L$) and circumferential strain estimation ($i = C$). The start and end of the cardiac cycle was manually identified as the time point with zero derivative before the largest positive derivative of the curve. This was done since it was not possible to use the ECG from the animal as input to the sonomicrometry system.

2.4. Statistical analysis

Peak systolic longitudinal and circumferential strain at baseline and hypertension averaged over three cardiac cycles estimated by speckle tracking was correlated with the reference strain by sonomicrometry using the Pearson correlation coefficient. Peak systolic strain values were also processed in a Bland–Altman analysis, where the bias was calculated as the difference between estimated and reference peak strain values ($\hat{\varepsilon}_{peak} - \varepsilon_{peak}$) averaged over the acquisitions at baseline and hypertension in all sheep. The root mean square error (RMSE) between reference and estimated strains throughout the first cardiac cycle was calculated as:

$$\text{RMSE} = \sqrt{\sum_{t=1}^{T} \frac{(\varepsilon(t) - \hat{\varepsilon}(t))^2}{T}}, \tag{3}$$

where $\hat{\varepsilon}(t)$ was the estimated strain, $\varepsilon(t)$ the reference strain and T the number of frames in one cycle. A *t*-test was used to test if there was a significant bias and RMSE in the estimations. *P*-values lower or equal to 0.05 were considered significant.

In addition, the variability in longitudinal and circumferential peak strain over time was calculated as the relative mean difference (RMD) between the three peak systolic strain values as:

$$\text{RMD} = \frac{(|\hat{\varepsilon}_1 - \hat{\varepsilon}_2| + |\hat{\varepsilon}_1 - \hat{\varepsilon}_3| + |\hat{\varepsilon}_2 - \hat{\varepsilon}_3|)}{3 \times \varepsilon} \times 100, \tag{4}$$

where $\hat{\varepsilon}_1$, $\hat{\varepsilon}_2$ and $\hat{\varepsilon}_3$ was estimated peak systolic strain for each of the three cardiac cycles and ε the peak systolic reference strain (averaged over six cycles).

Table 2. Peak systolic strain values estimated by speckle tracking in the left common carotid artery wall before exposing the artery (unexposed) at baseline and after exposing the artery and attaching sonomicrometry crystals (exposed) at baseline and hypertension.

	Unexposed	Exposed	
	Baseline	Baseline	Hypertension
Longitudinal strain (%)	2.30 (0.63)	0.78 (0.24)	1.25 (0.58)
Circumferential strain (%)	2.73 (0.71)	0.97 (0.34)	1.35 (0.66)
Radial strain (%)	−5.47 (1.65)	−2.74 (1.16)	−4.23 (1.81)

Strain values are presented as mean (SD) of three consecutive cardiac cycles from measurements in four sheep (longitudinal, circumferential and radial strain in unexposed artery and circumferential strain in exposed artery) and five sheep (longitudinal and radial strain in exposed artery).

3. Results

The heart rate was 70 ± 4 beats per minute and 143 ± 57 beats per minute and the systolic/diastolic blood pressure was 82 ± 8 / 63 ± 11 mmHg and 166 ± 30 / 120 ± 33 mmHg at baseline and hypertension, respectively. The estimated longitudinal, circumferential and radial strain curves varied cyclically throughout the cardiac cycle, showing a longitudinal and circumferential lengthening and radial thinning of the arterial segment in systole. Figures 3–5 show example longitudinal, circumferential and radial strain curves from three of the sheep. Peak systolic strain values in the unexposed and exposed artery are presented in table 2.

Circumferential strain estimation in the exposed artery of one sheep (sheep #4) was excluded from the analysis since the circumferential motion of the artery was very small and difficult to assess with both sonomicrometry and speckle tracking. Strain could also not be estimated in one sheep (sheep #2) before exposure and only throughout two cardiac cycles in the ultrasound short-axis acquisitions in sheep #3 (figure 4), because of corrupted ultrasound images in the storage procedure.

The estimated longitudinal and circumferential strain corresponded well with reference strain acquired by sonomicrometry. Table 3 presents bias, RMD and RMSE for longitudinal and circumferential strain estimation, whereas correlation and Bland–Altman plots are shown in figure 6. The limits of agreement were −0.15 to 0.42% and −0.54 to 0.50% for longitudinal and circumferential strain estimation, respectively. Significant correlations between peak systolic estimated and reference strain was found longitudinally ($r = 0.95$, $p < 0.001$) and circumferentially ($r = 0.87$, $p < 0.01$). RMSEs differed significantly from zero for both longitudinal and circumferential strain estimation ($p < 0.001$), whereas a significant bias (overestimation) in peak strain was found only for longitudinal strain estimation ($p < 0.05$). Estimated radial strain curves could not be compared with reference strain since no crystal was attached to the artery wall in the lumen. Nevertheless, radial strain profiles were physiological (figure 5) and in the same range with slightly higher amplitude than longitudinal and circumferential strain.

The obtained strain values had slightly higher amplitude during hypertension compared to baseline, which is illustrated in figures 4–6 and in table 2. Moreover, measured arterial strain amplitude was higher before exposing the artery than after attaching the sonomicrometry crystals as presented in table 2 and illustrated in the strain curves from one of the sheep in figure 7.

Table 3. Bias, RMD and RMSE of strain estimation by speckle tracking in the left common carotid artery using sonomicrometry strain as reference.

	Longitudinal strain	Circumferential strain
Bias (%)	0.14 (0.14)*	−0.02 (0.27)
RMD (%)	27 (12)	31 (28)
RMSE (%)	0.26 (0.07)**	0.29 (0.12)**

*$p < 0.05$; **$p < 0.001$.
The values are expressed as mean (SD) of three consecutive cardiac cycles of measurements in five sheep (longitudinal strain) and four sheep (circumferential strain). The RMSEs differed significantly from zero for both longitudinal and circumferential strain estimation, whereas the bias differed significantly from zero only for longitudinal strain estimation.
RMD: relative mean difference, RMSE: root mean square error, SD: standard deviation.

4. Discussion

This study investigated the feasibility of ultrasound-based strain assessment in the carotid artery wall by contrasting strain estimated by ultrasound speckle tracking with strain obtained by sonomicrometry in a sheep model. The results of the validation imply that strain assessment in the carotid artery wall *in-vivo* using ultrasound speckle tracking is feasible. Speckle tracking and sonomicrometry strain agreed, since acceptable limits of agreement (longitudinally: −0.15 to 0.42%, circumferentially: −0.54 to 0.50%) and low bias (longitudinally: 0.14 ± 0.14%, circumferentially: −0.02 ± 0.27%) were found. The feasibility was further demonstrated by strong correlations between speckle tracking and sonomicrometry strain, $r = 0.95$, $p < 0.001$ (longitudinally) and $r = 0.87$, $p < 0.01$ (circumferentially), figure 6.

The results of this study confirm previous validation studies demonstrating the feasibility to estimate strain of the carotid artery *in-silico* (Hansen *et al* 2009, Lopata *et al* 2009, Larsson *et al* 2011) and *in-vitro* (Ribbers *et al* 2007, Hansen *et al* 2009, Larsson *et al* 2015). However, results from strain estimation in simulated data sets and in gel phantoms cannot directly be translated to the more challenging *in-vivo* setting. Although arterial strain has previously been assessed *in-vivo* (Maurice *et al* 2008, Kawasaki *et al* 2009, Bjallmark *et al* 2010, Catalano *et al* 2011, McCormick *et al* 2012, Saito *et al* 2012), a thorough *in-vivo* validation study of arterial strain assessment by ultrasound speckle tracking via an independent method has to the authors´ knowledge been missing. In some of the mentioned studies, commercial speckle tracking algorithms originally developed for cardiac strain assessment have been applied. However, cardiac strain tracking cannot be considered equivalent to vascular strain tracking, since both dimensions and motion patterns are very different from the vascular setting. Even though the in-house algorithm used in this study is based on the same block-matching principle as many of the commercial algorithms, the advantage of the proposed algorithm is that the motion estimation parameters have been tuned for vascular applications and validated both *in-silico* (Larsson *et al* 2011) and *in-vitro* (Larsson *et al* 2015).

The strain amplitudes obtained in the present animal model were considerably lower than in our previous validation setups, which consisted of simulated kinematic models (Larsson *et al* 2011) and dynamic gel phantoms mimicking the carotid artery (Larsson *et al* 2015). As a result, the estimation errors in the present validation were smaller compared with the ones previously obtained *in-silico* and *in-vitro,* although this was not the case when considering the errors in relation to the estimated strain amplitudes in the different settings. A poorer performance of the speckle tracking analysis was expected in the *in-vivo* validation, since this setting to a larger extent mimicked the clinical *in-vivo* setting imposing more imaging artefacts. Furthermore, the use of sonomicrometry as reference method was more demanding in

the animal model than in the phantoms in terms of crystal attachment and signal acquisition. Despite these limitations, the obtained agreement between speckle tracking and sonomicrometry strain in this more challenging validation setting further strengthens the feasibility of strain assessment in the carotid artery wall.

A limitation with the present study is the lack of reference radial strain. This could possibly have been achieved by inserting a sonomicrometry crystal in the lumen and attaching it to the intima opposite the crystals attached to the adventitia. This intervention was however not included in the experimental protocol, since it would have been difficult to perform and since a puncture of the artery most likely would have altered the artery wall motion pattern considerably. Although no comparison with sonomicrometry strain was accomplished, radial strain estimated by speckle tracking indicated the feasibility of radial strain assessment *in-vivo*. The feasibility was supported by demonstrating physiological radial strain curves that cyclically varied over three cardiac cycles (figure 5) and resembled strain curves previously found *in-vivo* (Kawasaki *et al* 2009). However, in an incompressible material, and assuming that the strain is sufficiently small (orders of 1%), the sum of the strain components along the different axes is expected to be close to zero. A possible reason to why this was not the case in the present study is that the strain components were assessed in two imaging planes in slightly different regions of the arterial wall.

In this study, the investigated arterial segment showed a longitudinal lengthening in systole, which is in concordance with previous results from video microscopy in rats (Lichtenstein *et al* 1995) but contradictive to a previous study using sonomicrometry in a porcine model (Tozzi *et al* 2001). In the latter, a shortening of the carotid artery in systole was demonstrated. Differences in experimental conditions and procedures to attach the crystals are probable reasons to the differing findings. Similar to Tozzi *et al*, during initial testing of the present animal setup, shortening of the arterial segment was observed as a consequence of a lengthy surgical procedure when exposing the artery and stitching the crystals on the adventitia. Consequently, for the animals in this study, careful attention was paid to not affect the deformation pattern of the artery during surgery in order to achieve a similar deformation pattern as at baseline before exposure. In agreement with previous studies (Kawasaki *et al* 2009, Catalano *et al* 2011), radial strain was negative, demonstrating a systolic thinning of the arterial wall, whereas circumferential strain was positive, demonstrating a diameter increase in systole.

The carotid strain amplitudes in the studied animal model were lower than previously observed *in-vivo* in humans (Bjallmark *et al* 2010, Catalano *et al* 2011). Some probable reasons for the low strain amplitudes in the animal model might be differences in human and sheep physiology, the surgical intervention, drug administration and the stretched neck posture of the animals. It is likely that the anesthesia caused a low pulse pressure due to vasodilation, which in turn resulted in low strain amplitudes. Moreover, phenylephrine may have caused smooth muscle cell contraction in the media layer of the artery, which could also be a cause of the decreased strain amplitudes. The surgical exposure seemed to have an effect on the carotid strain pattern in the model, resulting in decreased strain in the exposed artery compared to the unexposed artery as illustrated in figure 7. This may have been a result of surrounding tissue removal or a change in elastic properties although the adventitia was left in place and attention was paid not to damage the adventitia when suturing the crystals. Vascular spasm may also have affected the observed change in carotid strain pattern. However, the strain range obtained in this study was considered to be sufficient for validation, which was confirmed by the promising results. Moreover, assessment of higher strain values in clinical practice compared to the ones obtained in this validation study may be easier, since low inter-frame displacements close to sub-pixel level as encountered in this validation setup are more difficult to track.

Drug administration for induction of hypertension may have affected the carotid strain pattern in terms of vasoconstriction. Hypertension was induced to alter the arterial strain pattern in order to obtain a larger range of strain values for the validation. However, hypertension did not increase arterial strain consistently (figures 3 and 4). The administration of an alternative drug to induce hypertension may have induced larger longitudinal strains than Phenylephrine, since arterial longitudinal motion has showed to increase in response to catecholamines (Ahlgren *et al* 2012). However, the inner-most layer of the artery wall increased more in longitudinal motion than the adventitia, resulting in an increased longitudinal shear strain. This indicates that administration of catecholamines instead of Phenylephrine, may not have induced larger strains in this animal model since the crystals were sutured on the adventitia and not on the inner-most layer of the artery.

A common source of error in ultrasound speckle tracking is speckle decorrelation due to out-of-plane motion and tissue compression. It is also worthwhile emphasizing the limitation of using sonomicrometry as reference method, since its accuracy is limited in terms of spatial resolution when measuring such small distances. Although careful attention was paid to position the crystals for circumferential strain calculation in the same cross-section, this was not always achieved due to difficulties in the stitching procedure. Crystal positioning off the circumferential axis was however small (1–2 mm in the axis along the vessel) and not considered to have a major influence on the results. Moreover, sonomicrometry and speckle tracking circumferential strain were obtained using two slightly different approaches. Sonomicrometry circumferential strain was derived from the diameter change in the short-axis view, since the diameter of the artery is proportional to its circumference, whereas circumferential strain by speckle tracking was assessed in a circular ROI positioned in the middle of the arterial wall at 3 o'clock with a circumferential ROI size of 90°. This approach of assessing reference circumferential strain was selected since a too small inter-crystal distance was not feasible because of the dimensions of the crystals and vessel. Further, this approach assumed an evenly distributed circumferential strain, which does not account for e.g. differences in surrounding tissues.

Another factor that could have influenced the discrepancy between the methods was slightly different measurement sites, which was necessary in order to avoid interference of the crystals in the tracking process. The longitudinal strain was slightly overestimated ($p < 0.001$, bias = 0.14%), which may be a result of a strain gradient across the wall and the attachment of the crystals on the adventitia, whereas the ROI for speckle tracking estimation mainly covered the intima-media complex. A similar result was expected for circumferential strain estimation, but the bias for strain in this direction was not significant. In contrast to sonomicrometry, speckle tracking showed lower longitudinal strain values at hypertension than baseline in sheep #2 (figure 3). Sonomicrometry strain is obtained at the same site at baseline and hypertension, since the crystals are fixed on the artery. Speckle tracking strain, however, may be obtained from slightly different sites as the transducer is hand-held and the ROI is positioned manually in the wall. This may be one reason for this contradicting result. Other reasons may be poor performance of the speckle tracking algorithm due to decorrelation caused by e.g. out of plane motion.

The heart rate and blood pressure of the sheep rapidly changed when inducing hypertension. In some animals, this led to acquisition of sonomicrometry and ultrasound data in slightly different physiological conditions. However, the difference in physiological conditions between acquisition of sonomicrometry and ultrasound data was small and considered to have low impact on the validation results. In addition, the animals responded differently to Phenylephrine, which made the level of hypertension difficult to standardize. On the other hand, this was not significant for the validation study since the purpose of inducing hypertension was to obtain a range of strain values for the validation rather than achieving similar
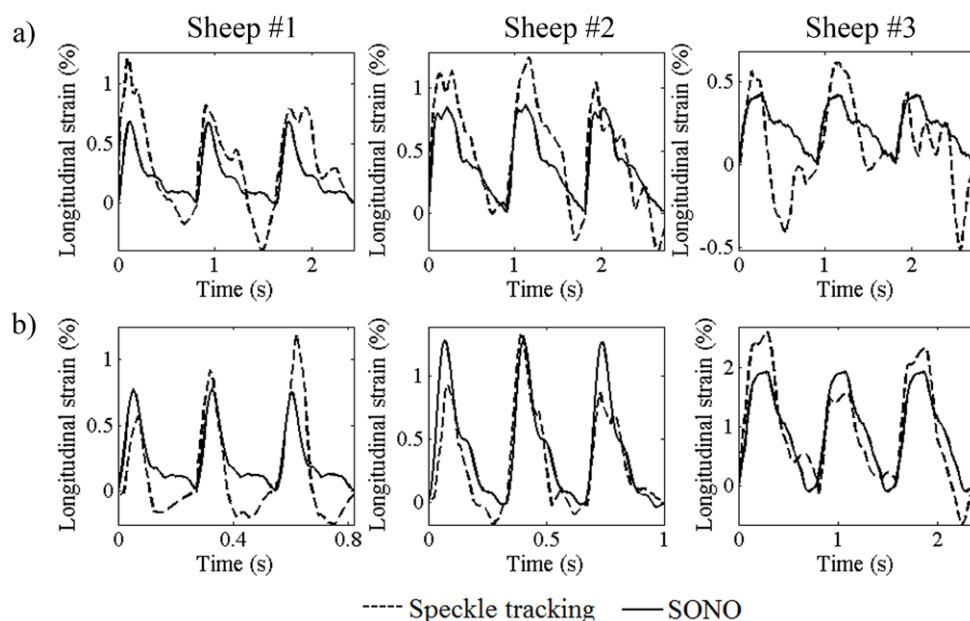
Figure 3. Example longitudinal strain curves from the left common carotid artery in three of the sheep throughout three consecutive cardiac cycles estimated by ultrasound speckle tracking and SONO at baseline (*a*) and hypertension (*b*). SONO: sonomicrometry.

levels of hypertension in all animals. The frame rate of ultrasound imaging was not adapted for heart rate, which resulted in a difference in inter-frames displacements at hypertension and baseline that may have affected the tracking quality. However, no obvious difference in performance at baseline and hypertension was observed in this study (figures 3 and 4).

The application of the presented speckle tracking algorithm in clinical use is strongly dependent on image quality and minimization of out-of plane motion due to patient and transducer movement. In comparison with commercially available echo-tracking methods based on measurement of pressure and diameter changes (Niki *et al* 2002, Tanaka *et al* 2013), the speckle tracking method offers advantages of assessing mechanical properties in a small ROI inside the arterial wall. As such, a more local measure of arterial stiffness may be achieved and e.g. stiffness of different arterial layers and in different wall directions as well as shear stiffness can be studied. Further, the clinical applicability of the speckle tracking method can be discussed by relating the accuracy of the method to clinically relevant differences in arterial strain values. Previous studies have observed differences of approximately 4% in circumferential strain between young and old healthy subjects (Bjallmark *et al* 2010, Yuda *et al* 2011), whereas radial strain differed up to 10% between patients with coronary artery disease and healthy control subjects (Kawasaki *et al* 2009). Although the strain amplitudes in the current study were considerably lower than the ones found in these studies, our findings indicate that the proposed algorithm has potential to detect clinical relevant differences in strain. Furthermore, the relative high variability in strain values over consecutive cardiac cycles (> 27%) obtained in this study stresses the importance of repeated arterial strain measurements in future studies. Repeated measurements at different spatial locations would most probably result in a more robust estimation of arterial strain.
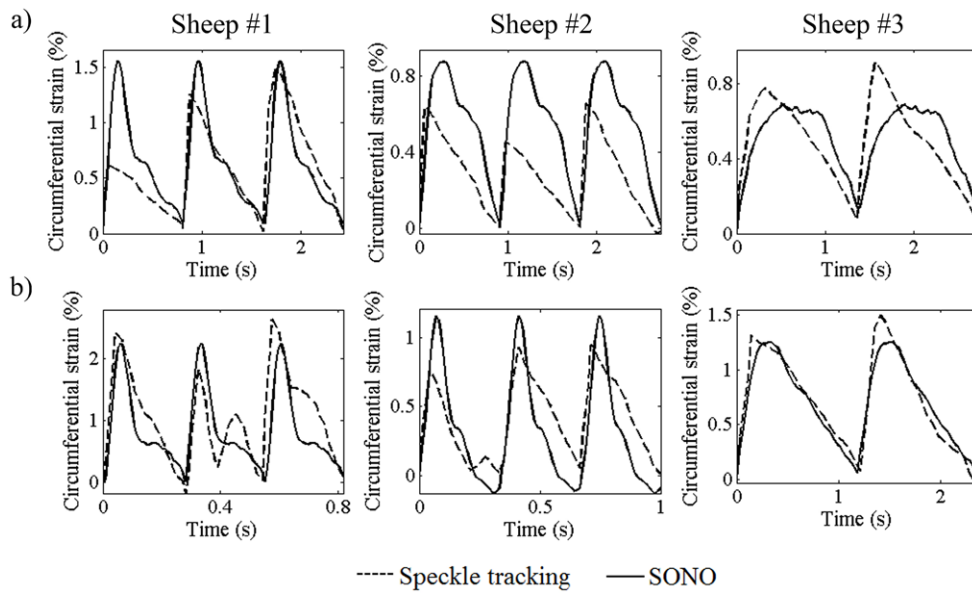
Figure 4. Example circumferential strain curves from the left common carotid artery wall in three of the sheep estimated by ultrasound speckle tracking and SONO at baseline (*a*) and hypertension (*b*). SONO: sonomicrometry.
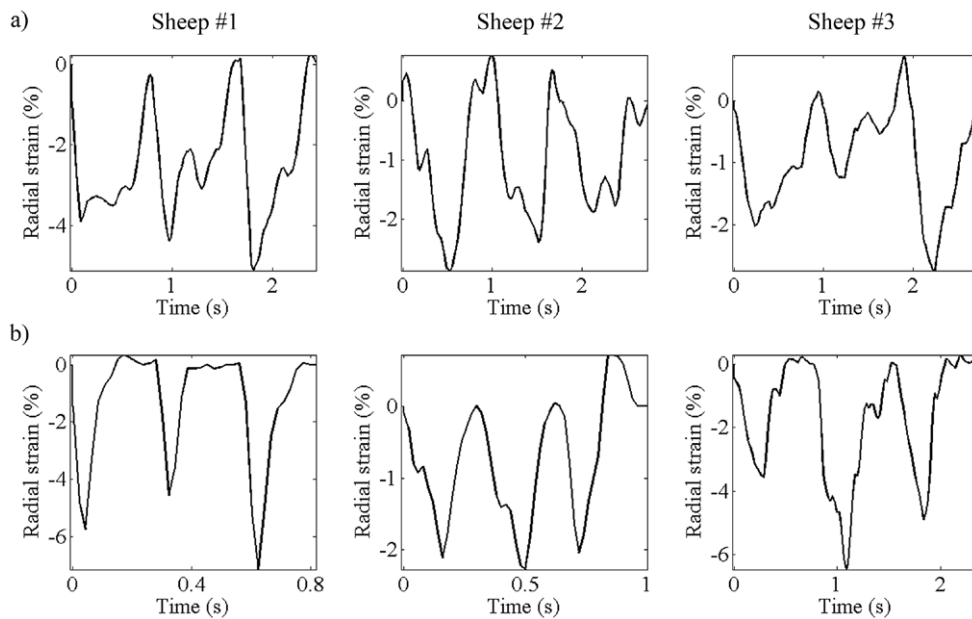

Figure 5. Example radial strain curves from the left common carotid artery wall in three of the sheep throughout three consecutive cardiac cycles estimated by ultrasound speckle tracking at baseline (*a*) and hypertension (*b*).
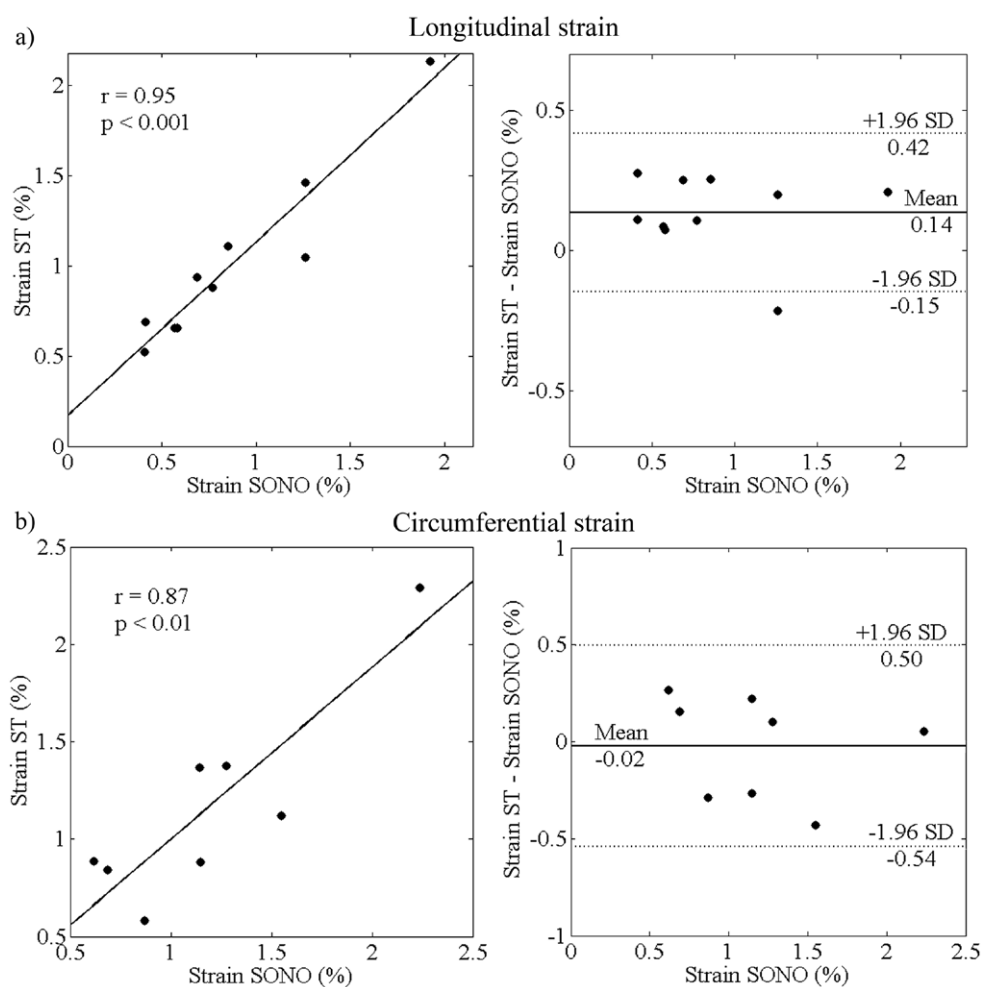
Figure 6. Correlation plots (left) and Bland–Altman plots (right) of peak systolic longitudinal strain (*a*) and circumferential strain (*b*) in the left carotid artery wall by SONO and ST (mean of three cardiac cycles) at baseline and hypertension in five sheep for longitudinal strain estimation (*n* = 10) and four sheep for circumferential strain estimation (*n* = 8). ST: speckle tracking, SONO: sonomicrometry.

At present, several studies regarding arterial strain assessment *in-vivo* have been carried out (Maurice *et al* 2008, Kawasaki *et al* 2009, Bjallmark *et al* 2010, Catalano *et al* 2011, McCormick *et al* 2012, Saito *et al* 2012) but there are no larger clinical studies assessing arterial strain. In particular, the number of studies describing longitudinal strain of the arterial wall is limited. Further studies are required to determine the clinical value of arterial longitudinal motion and strain although initial results show that the longitudinal function may be an early marker of cardiovascular disease (Zahnd *et al* 2012), is associated with plaque burden (Svedlund and Gan 2011) and has potential to predict cardiovascular outcome (Svedlund *et al* 2011). Moreover, arterial longitudinal shear strain is considered to stimulate development of rupture-prone plaques (Idzenga *et al* 2012). Still, the feasibility of arterial strain assessment to perform cardiovascular risk stratification in order to assess the presence of subclinical
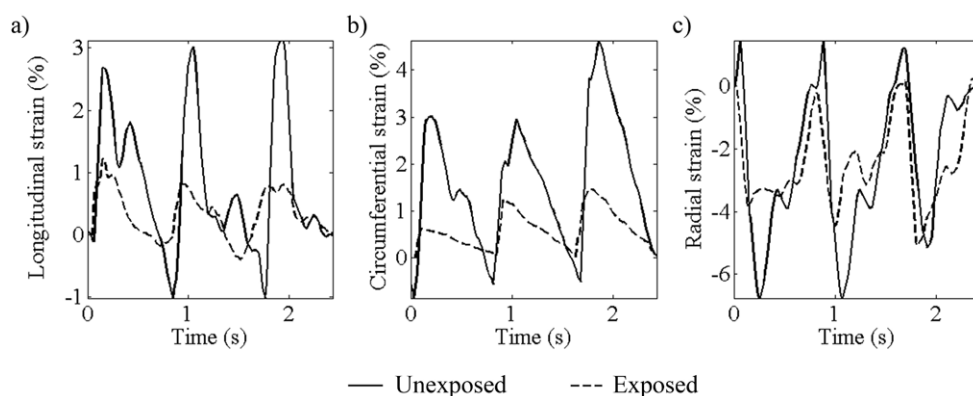
Figure 7. (*a*) Longitudinal, (*b*) circumferential and (*c*) radial strain curves from the left common carotid artery wall in one of the sheep (sheep #1) at baseline before exposure (solid line) and after exposure and attachment of sonomicrometry crystals (dashed line) estimated by ultrasound speckle tracking throughout three consecutive cardiac cycles.

cardiovascular disease and characterize atherosclerotic plaques needs to be further investigated *in-vivo* and the method needs to be compared with existing methods.

5. Conclusion

The results from this validation study demonstrate the feasibility of arterial strain assessment *in-vivo* using ultrasound speckle tracking. However, the feasibility of assessing strain of the human carotid artery using ultrasound speckle tracking needs to be further investigated along with the potential of the method to estimate arterial stiffness and characterize atherosclerotic plaques.

Acknowledgement

References

Ahlgren A R, Cinthio M, Steen S, Nilsson T, Sjoberg T, Persson H W and Lindstrom K 2012 Longitudinal displacement and intramural shear strain of the porcine carotid artery undergo profound changes in response to catecholamines *Am. J. Physiol. Heart Circ. Physiol.* **302** H1102–15
Bjallmark A, Lind B, Peolsson M, Shahgaldi K, Brodin L A and Nowak J 2010 Ultrasonographic strain imaging is superior to conventional non-invasive measures of vascular stiffness in the detection of age-dependent differences in the mechanical properties of the common carotid artery *Eur. J. Echocardiogr.* **11** 630–6
Catalano M, Lamberti-Castronuovo A, Catalano A, Filocamo D and Zimbalatti C 2011 2D speckle-tracking strain imaging in the assessment of mechanical properties of carotid arteries: feasibility and comparison with conventional markers of subclinical atherosclerosis *Eur. J. Echocardiogr.* **12** 528–35

Cinthio M, Ahlgren A R, Bergkvist J, Jansson T, Persson H W and Lindstrom K 2006 Longitudinal movements and resulting shear strain of the arterial wall *Am. J. Physiol. Heart Circ. Physiol.* **291** H394–402

Cinthio M, Ahlgren A R, Jansson T, Eriksson A, Persson H W and Lindstrom K 2005 Evaluation of an ultrasonic echo-tracking method for measurements of arterial wall movements in 2D *IEEE Trans. Ultrason. Ferroelectr. Freq. Control* **52** 1300–11

D'hooge J, Konofagou E, Jamal F, Heimdal A, Barrios L, Bijnens B, Thoen J, Van de Werf F, Sutherland G and Suetens P 2002 2D ultrasonic strain rate measurement of the human heart *in vivo IEEE Trans. Ultrason. Ferroelectr. Freq. Control* **49** 281–6

de Korte C L, Sierevogel M J, Mastik F, Strijder C, Schaar J A, Velema E, Pasterkamp G, Serruys P W and van der Steen A F 2002 Identification of atherosclerotic plaque components with intravascular ultrasound elastography *in vivo*: a Yucatan pig study *Circulation* **105** 1627–30

Eryol N K, Topsakal R, Ciçek Y, Abaci A, Oguzhan A, Basar E and Ergin A 2002 Color Doppler tissue imaging in assessing the elastic properties of the aorta and in predicting coronary artery disease *Japan. Heart J.* **43** 219–30

Falk E, Shah P K and Fuster V 1995 Coronary plaque disruption *Circulation* **92** 657–71

Fleiner M, Kummer M, Mirlacher M, Sauter G, Cathomas G, Krapf R and Biedermann B C 2004 Arterial neovascularization and inflammation in vulnerable patients: early and late signs of symptomatic atherosclerosis *Circulation* **110** 2843–50

Golemati S, Sassano A, Lever M J, Bharath A A, Dhanjil S and Nicolaides A N 2003 Carotid artery wall motion estimated from B-mode ultrasound using region tracking and block matching *Ultrasound Med. Biol.* **29** 387–99

Hae Guen S, Eung Ju K, Hong Seog S, Seong Hwan K, Chang Gyu P, Seong Woo H and Ryu K H 2010 Relative contributions of different cardiovascular risk factors to significant arterial stiffness *Int. J. Cardiol.* **139** 263–8

Hansen H H, Lopata R G and de Korte C L 2009 Noninvasive carotid strain imaging using angular compounding at large beam steered angles: validation in vessel phantoms *IEEE Trans. Med. Imaging* **28** 872–80

Hermeling E, Reesink K, Reneman R and Hoeks A 2007 Measurement of local pulse wave velocity: effects of signal processing on precision *Ultrasound Med. Biol.* **33** 774–81

Hoeks A, Brands P, Smeets F and Reneman R 1990 Assessment of the distensibility of superficial arteries *Ultrasound Med. Biol.* **16** 121–8

Idzenga T, Hansen H, Lopata R and de Korte C 2012 Estimation of longitudinal shear strain in the carotid arterial wall using ultrasound radiofrequency data *Ultraschall in der Medizin* **33** E275–82

Kawasaki T *et al* 2009 Direct measurement of wall stiffness for carotid arteries by ultrasound strain imaging *J. Am. Soc. Echocardiogr.* **22** 1389–95

Korstanje J W, Selles R W, Stam H J, Hovius S E and Bosch J G 2010 Development and validation of ultrasound speckle tracking to quantify tendon displacement *J. Biomech.* **43** 1373–9

Korukonda S and Doyley M M 2012 Visualizing the radial and circumferential strain distribution within vessel phantoms using synthetic-aperture ultrasound elastography *IEEE Trans. Ultrason. Ferroelectr. Freq. Control* **59** 1639–53

Kremer F, Choi H F, Langeland S, D'Agostino E, Claus P and D'Hooge J 2010 Geometric regularization for 2D myocardial strain quantification in mice: an in-silico study *Ultrasound Med. Biol.* **36** 1157–68

Larsson M, Heyde B, Kremer F, Brodin L K and D'Hooge J 2015 Ultrasound speckle tracking for radial, longitudinal and circumferential strain estimation of the carotid artery—an *in vitro* validation via sonomicrometry using clinical and high-frequency ultrasound *Ultrasonics* **56** 399–408

Larsson M, Kremer F, Claus P, Kuznetsova T, Brodin L A and D'Hooge J 2011 Ultrasound-based radial and longitudinal strain estimation of the carotid artery: a feasibility study *IEEE Trans. Ultrason. Ferroelectr. Freq. Control* **58** 2244–51

Liang Y, Zhu H and Friedman M H 2009 The correspondence between coronary arterial wall strain and histology in a porcine model of atherosclerosis *Phys. Med. Biol.* **54** 5625–41

Lichtenstein O, Safar M E, Poitevin P and Levy B I 1995 Biaxial mechanical properties of carotid arteries from normotensive and hypertensive rats *Hypertension* **26** 15–9

Lopata R G, Nillesen M M, Hansen H H, Gerrits I H, Thijssen J M and de Korte C L 2009 Performance evaluation of methods for 2D displacement and strain estimation using ultrasound radio frequency data *Ultrasound Med. Biol.* **35** 796–812

Mahmoud A, Frisbee J, D'Audiffret A and Mukdadi O 2009 *In vivo* vascular wall tissue characterization using a strain tensor measuring (STM) technique for flow-mediated vasodilation analyses *Phys. Med. Biol.* **54** 6217–38

Maurice R L, Soulez G, Giroux M F and Cloutier G 2008 Noninvasive vascular elastography for carotid artery characterization on subjects without previous history of atherosclerosis *Med. Phys.* **35** 3436–43

McCormick M, Varghese T, Wang X, Mitchell C, Kliewer M A and Dempsey R J 2012 Methods for robust *in vivo* strain estimation in the carotid artery *Phys. Med. Biol.* **57** 7329–53

Naghavi M *et al* 2003 From vulnerable plaque to vulnerable patient: a call for new definitions and risk assessment strategies: I *Circulation* **108** 1664–72

NASCET 1991 North American Symptomatic Carotid Endarterectomy Trial. Methods, patient characteristics, and progress *Stroke* **22** 711–20

Niki K, Sugawara M, Chang D, Harada A, Okada T, Sakai R, Uchida K, Tanaka R and Mumford C E 2002 A new noninvasive measurement system for wave intensity: evaluation of carotid arterial wave intensity and reproducibility *Heart Vessels* **17** 12–21

Persson M, Ahlgren A R, Jansson T, Eriksson A, Persson H W and Lindstrom K 2003 A new non-invasive ultrasonic method for simultaneous measurements of longitudinal and radial arterial wall movements: first *in vivo* trial *Clin. Physiol. Funct. Imaging* **23** 247–51

Redheuil A, Wen-Chung Y, Wu C, Mousseaux E, de Cesare A, Yan R, Kachenoura N, Bluemke D and Lima J 2010 Reduced ascending aortic strain and distensibility: earliest manifestations of vascular aging in humans *Hypertension* **55** 319–26

Ribbers H, Lopata R, Holewijn S, Pasterkamp G, Blankensteijn J and de Korte C 2007 Noninvasive 2D strain imaging of arteries: validation in phantoms and preliminary experience in carotid arteries *in vivo Ultrasound Med. Biol.* **33** 530–40

Saito M, Okayama H, Inoue K, Yoshii T, Hiasa G, Sumimoto T, Nishimura K, Ogimoto A and Higaki J 2012 Carotid arterial circumferential strain by 2D speckle tracking: a novel parameter of arterial elasticity *Hypertension Res.* **35** 897–902

Schmitt C, Soulez G, Maurice R, Giroux M and Cloutier G 2007 Noninvasive vascular elastography: toward a complementary characterization tool of atherosclerosis in carotid arteries *Ultrasound Med. Biol.* **33** 1841–58

Staub D *et al* 2010 Contrast-enhanced ultrasound imaging of the vasa vasorum: from early atherosclerosis to the identification of unstable plaques *JACC Cardiovasc. Imaging* **3** 761–71

Sutton-Tyrrell K *et al* 2005 Elevated aortic pulse wave velocity, a marker of arterial stiffness, predicts cardiovascular events in well-functioning older adults *Circulation* **111** 3384–90

Svedlund S, Eklund C, Robertsson P, Lomsky M and Gan L M 2011 Carotid artery longitudinal displacement predicts 1 year cardiovascular outcome in patients with suspected coronary artery disease *Arterioscler. Thromb. Vasc. Biol.* **31** 1668–74

Svedlund S and Gan L M 2011 Longitudinal common carotid artery wall motion is associated with plaque burden in man and mouse *Atherosclerosis* **217** 120–4

Tanaka M, Sugawara M, Ogasawara Y, Izumi T, Niki K and Kajiya F 2013 Intermittent, moderate-intensity aerobic exercise for only eight weeks reduces arterial stiffness: evaluation by measurement of stiffness parameter and pressure-strain elastic modulus by use of ultrasonic echo tracking *J. Med. Ultrason.* **40** 119–24

Tozzi P, Hayoz D, Oedman C, Mallabiabarrena I and Von Segesser L K 2001 Systolic axial artery length reduction: an overlooked phenomenon in vivo *Am. J. Physiol. Heart Circ. Physiol.* **280** H2300–5

Yuda S, Kaneko R, Muranaka A, Hashimoto A, Tsuchihashi K, Miura T, Watanabe N and Shimamoto K 2011 Quantitative measurement of circumferential carotid arterial strain by 2D speckle tracking imaging in healthy subjects *Echocardiography* **28** 899–906

Yusuf S *et al* 2004 Effect of potentially modifiable risk factors associated with myocardial infarction in 52 countries (the INTERHEART study): case-control study *Lancet* **364** 937–52

Zahnd G *et al* 2012 Longitudinal displacement of the carotid wall and cardiovascular risk factors: associations with aging, adiposity, blood pressure and periodontal disease independent of cross-sectional distensibility and intima-media thickness *Ultrasound Med. Biol.* **38** 1705–15